

Fragility of Older-vintage Continuous California Bridges to Liquefaction and Lateral Spreading

Pirooz Kashighandi¹, Scott J. Brandenburg², Jian Zhang³, Yili Huo⁴, and Minxing Zhao⁵

¹ Graduate Student, Department of Civil and Environmental Engineering, University of California, 5731 Boelter Hall, Los Angeles, CA 90095-1593, pirooz@ucla.edu

² Assistant Professor, Department of Civil and Environmental Engineering, University of California 5731 Boelter Hall, Los Angeles, CA 90095-1593, sjbrandenberg@ucla.edu

³ Assistant Professor, Department of Civil and Environmental Engineering, University of California, 5731 Boelter Hall, Los Angeles, CA 90095-1593, zhangj@ucla.edu

⁴ Graduate Student, Department of Civil and Environmental Engineering, University of California, 5731 Boelter Hall, Los Angeles, CA 90095-1593, huoyili@ucla.edu

⁵ Graduate Student, Department of Civil and Environmental Engineering, University of California, 5731 Boelter Hall, Los Angeles, CA 90095-1593, zhaomx@ucla.edu

ABSTRACT: Static pushover analyses are utilized to evaluate the vulnerability of typical older-vintage California bridges with continuous superstructures and monolithic abutments to liquefaction and lateral spreading. 950 Monte Carlo analyses with varying bridge structural properties and varying demands and displacement patterns were performed and damage to different components of the bridge and the fundamental failure mechanisms were identified. Global modeling of the bridge proved to be advantageous since some of the failure mechanisms identified in these analyses cannot be identified with component-wise local modeling of the bridge. Results of the analyses were also disaggregated with respect to their input parameters. The thickness of the nonliquefiable crust layer and strength (moment and shear capacity) of the piers were two of the most influential parameters in the performance of the bridge. Fragility curves representing free-field lateral spreading ground displacements required to exceed different levels of damage for this class of bridges were also presented.

KEYWORDS: Fragility Curves, Liquefaction, Lateral Spreading, Bridges

1. INTRODUCTION

California Department of Transportation (CALTRANS) owns over 13,000 bridges, most of which were constructed prior to a date when design codes contained any provisions for liquefaction, and therefore, it is uncertain how California's older bridges would perform in lateral spreading ground. Even after advances in earthquake engineering and implementation of seismic provisions in the design of the bridges, our knowledge of liquefaction and lateral spreading has been limited and therefore, the consequence of liquefaction and lateral spreading on bridges were not accounted for in the design of a majority of these bridges. In recent years, there have been major advances in understanding the liquefaction and lateral spreading and their demands on the structures and newer structures are designed with consideration of consequences of liquefaction and lateral spreading when the bridges are located in liquefiable soil profiles. However, the vulnerability of existing bridges to liquefaction and lateral spreading is unknown and thus needs to be evaluated. Since analyzing the entire suite of 13,000 bridges is not feasible, a two-step screening procedure is required to identify 1) whether or not the bridge is located in regions where liquefaction and lateral spreading might be expected to accompany earthquake shaking, and 2) how susceptible is the bridge, given the fact that it is located in regions where liquefaction and lateral spreading is likely to happen. The first criteria is dealt with in a separate Caltrans project by Keith Knudsen where the likelihood of liquefaction and lateral spreading at the bridge site is identified and also the extent of expected lateral spreading is estimated. This research focuses on the latter issue and intends to identify the vulnerability of different classes of existing bridges to liquefaction and lateral

spreading demands and identify the important parameters in the performance of the bridge, as well as the mechanisms of failure.

This paper's focus is on continuous multi-span bridges with monolithic abutments that were constructed prior to 1971, the year at which the occurrence of the San Fernando earthquake resulted in some major changes in seismic design codes. Since analyzing every bridge that belongs to this class is not feasible, the authors devised a method to account for variability in structural configurations, soil properties, and lateral spreading demands with a single 3-span bridge model template (Figure 1).

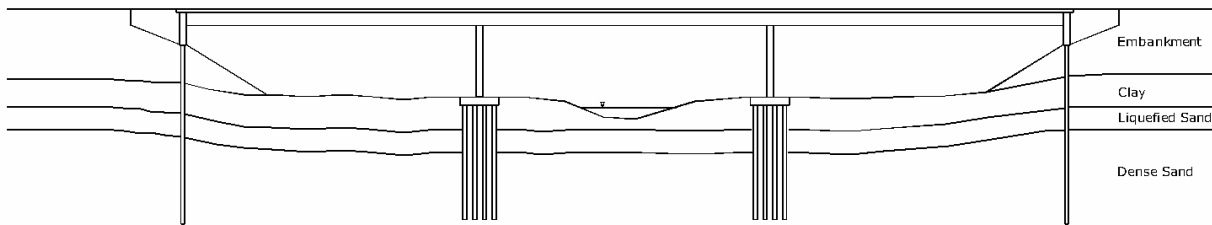


Figure 1: Schematic of the 3-span bridge model used in the analyses and the typical liquefied soil profile

The properties of the bridge, such as pier strength, span length and pier height, properties of the soil, such as embankment height, strength and thickness of the nonliquefied crust layer and liquefiable layer, and strength of the dense sand layer were varied in the analyses to represent variations in both the site and the bridge.

2. GLOBAL NUMERICAL ANALYSIS APPROACH

OpenSees finite element platform (Mazzoni et al., 2006) was used to model the entire structural components of the bridge and run the analyses. Global modeling of the bridge is preferable to modeling only the individual components of the bridge, because it can predict mechanisms of failure that could not be captured using component-wise modeling. Nonlinear beam column elements consisting of bilinear moment curvature, linear shear deformation, and linear axial force-deformation were used to model piers and piles. Linear beam column elements were used to model the superstructure deck, pile caps and abutment diaphragm walls.

P-y, t-z and q-z soil-structure elements were used to model the lateral, axial shaft friction and pile tip bearing soil-structure interaction effects, respectively. Properties of the p-y elements were computed based on median values of a typical liquefiable soil profile. The stiffness of the p-y elements in the nonliquefiable crust layer were softened following the models presented in Brandenberg et al. (2007) to account for the softening of the load transfer due to the existence of the underlying liquefied sand layer. The displacement demands on p-y elements in the nonliquefiable crust at both abutments were also accounted for the pinning effects at abutments (TRB 2002). The p-y elements in the liquefied sand layer were weakened by applying p-multipliers to account for liquefaction and reduction of effective stresses. The p-y elements on denser sandy soils underlying the liquefied sands were also weakened to a certain extent to account for generation of excess pore pressures. T-z shaft friction elements also had similar reductions in both the liquefied sand and dense sand layers to account for reduction of shaft friction as a result of ground shaking and liquefaction.

Displacements were applied at the free end of the p-y elements to model lateral spreading demands on piles and pile caps of the piers as well as the spreading demands on the diaphragm walls and the piles at the abutments. The soil displacement profile consisted of spreading with no strain in the nonliquefiable crust and large strains in the liquefied sand layer with a displacement discontinuity at the interface between the liquefied sand layer and the nonliquefied crust layer. No displacement existed in the dense sand layer underlying the liquefied sand layer. Inertia forces can occur simultaneously with lateral spreading forces and thus need to be modeled concurrently with lateral spreading. Therefore, inertia forces were applied on the superstructure as well as on the pile caps of the bridge concurrently with lateral spreading displacements.

Lateral spreading displacements are known to vary significantly throughout the spread feature (Faris 2004), so the amount of ground displacement imposed at each component was randomized to account for this inherent variability. Furthermore, 1/3 of the load cases involved lateral spreading only on the left side of the bridge (left abutment and the left intermediate pier), 1/3 with spreading only on the right side (right abutment and the right intermediate pier) and 1/3 with spreading on both sides. Spreading displacements within a spread feature (i.e. on one side of the bridge) were correlated. Ground displacements were increased linearly during the analyses while inertia loads were simultaneously increased. The maximum ground displacement imposed on any component was recorded as several engineering demand parameters (EDPs) exceeded various prescribed levels. EDPs included curvature ductility in the piers, shear force relative to shear capacity of the piers, displacement and rotation at each of the pile caps, displacement and rotation of the diaphragm wall at the abutments and curvature ductility in the piles at both the abutments and in the piers.

3. INPUT PARAMETERS

Monte Carlo analyses have been setup in such a way that all the input parameters of the analyses were sampled from realistic input distributions. Median value and variation (or standard deviation) of all of the parameters as well as their corresponding distributions are summarized in Table 1.

Table 1: Summary of the input parameters and their variations in the Monte Carlo analyses

Parameter	Median	Standard Deviation or Variation	Distribution
SpanLength ¹	21.6 m	13.3 m	Normal
Pier Height ²	6.5 m	1.65 m	Normal
Yield Moment of the Piers ³	4731 KN•m	$\sigma_{in} = 0.657$	Log-Normal
Shear Capacity of the Piers ⁴	1913 KN	$\sigma_{in} = 0.464$	Log-Normal
Natural Crust Thickness	3.0 m	0.0 to 6.0 m	Uniform
Embankment Thickness	6.0 m	3.0 to 9.0 m	Uniform
Liquefied Sand Thickness	3.0 m	$\sigma_{in} = 0.693$	Log-Normal
Natural Crust Material Properties	$\phi' = 38^\circ$ $c' = 20$ kPa $\gamma_{Embankment} = 20$ kN/m ³	$\sigma_{\phi'} = 5.7^\circ$ $\sigma_c = 10$ kPa	Log-Normal
Embankment Material Properties	$Su_{clay} = 70$ kPa $\gamma_{clay} = 9$ kN/m ³	$\sigma_{in}(Su_{clay}) = 0.7747$	Log-Normal
Top of Liq. Sand Disp. / Max. Crust Disp.	0.5	0.0 to 1.0	Uniform
Liquefied Sand Multiplier	0.05	0.025	Normal
Crust Stiffness (y_{50}) Multiplier	$y_{50abutment} = 0.20$ m $y_{50bent} = 0.05$ m	$\sigma_{y_{50abutment}} = 0.10$ m $\sigma_{y_{50bent}} = 0.025$ m	Normal
Axial Tip Capacity ⁵	1020 KN per pile	510 KN per pile	Normal
Inertia ⁶	$a_{peak} = 0.4g$ ⁷	0.2g	Normal

1 The distribution of the span length was truncated at 10 m at the lowerbound and at 60 m at the upperbound.

2 The distribution of the Pier Height was truncated at 2 m at the lowerbound and at 20 m at the upperbound.

3&4 Moment and Shear capacities of the piers were correlated with the span length of the bridge.

5 Skin Resistance Capacity was calculated depending on the soil profile properties and had the same variation as tip capacity.

6 Inertia load was applied in 50% of the analyses, due to the fact that sometimes lateral spreading occurs after ground shaking.

7 Inertia load was increased linearly with the ground displacement such that the peak acceleration was reached at 0.5m of ground displacement, after which was kept constant.

Selection of the distribution type and the variations of the parameters were based on data when available. For example, the median and standard deviation of the span lengths of the bridge were selected based on State of California's Pre-1971 bridges available in NBI (National Bridge Inventory) database of bridges, or the median and standard deviation of pier heights were selected based on available bridge drawings. However, when data was not available, the selection of input parameters was based on authors' best judgment.

4. SAMPLE ANALYSES

In this section, two cases of the Monte Carlo analyses are presented and the damage to different components of the bridge is discussed in detail.

Figure 2 shows the deformations at the end of the analysis of a bridge with 18.6m spans with pier yield moment of 5,740 kN·m and pier shear capacity of 2,472 kN but relatively short (4.43 m) piers. In this case, spreading is happening at both sides of the bridge with more spreading happening on the right side of the bridge and more displacements at the right abutment within the right spreading feature. No inertia force is applied in this case, which is typical of cases where lateral spreading occurs after ground shaking. The natural nonliquefied crust is 2.5m thick while the liquefied sand is 1.6 m thick.

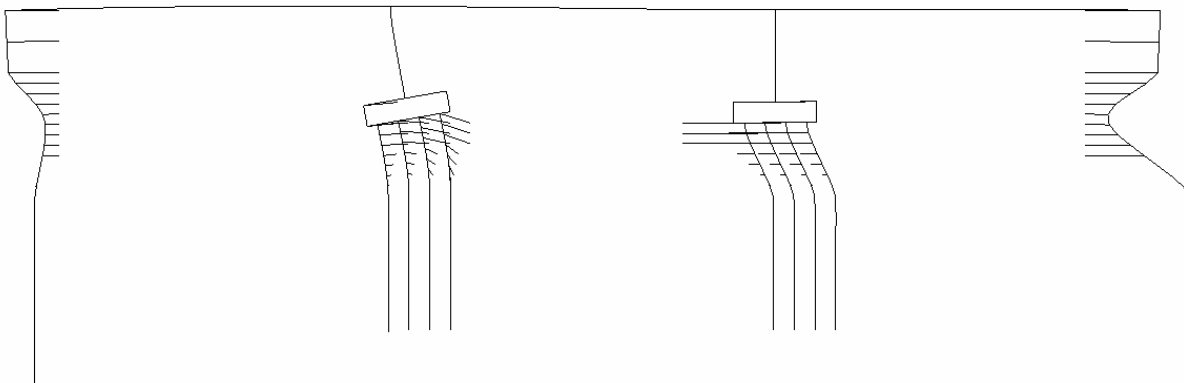


Figure 2: Deformations at the end of an analysis with moderately strong piers and spreading occurring on both sides (deformations are amplified by a factor of 10.0).

As can be observed in Figure 2, due to the fact that more lateral spreading is happening at the right side of bridge, the entire bridge is moving about 150mm to the left. Since there is significant spreading at the right pier, the pile cap at the right pier is also moving just over 150mm to the left by the end of the analysis. As a result no significant curvature is mobilized in the right pier despite about 0.80 m of ground displacement at the end of the analysis. However, the 0.40m-diameter piles supporting the right pier have reached a curvature ductility of 7 at the end of analysis.

On the other hand, the pile cap supporting the left pier moved only about 75mm from right to left while the fairly rigid superstructure moved 150mm from right to left, causing a significant displacement demand on the left pier. A large curvature ductility ($\mu_\phi = 7$) was mobilized in the left pier. One interesting feature in this analysis is that the pile cap supporting the left pier is rotating about 1.5 % counter-clockwise because of the translational movement of the entire bridge. It should also be noted that the counter-clockwise rotation of the pile cap is relieving the curvature demand on the left pier, which would have reached a large curvature ductility at a much lower ground displacement had the pile cap been fixed against rotation.

Figure 3 shows the deformations at the end of the analysis of a bridge with 36.1m spans and strong (pier yield moment = 19,500 kN·m; pier shear capacity = 3,950 kN) 9.95m-long tall piers. Spreading in this analysis, is happening only on the right side of the bridge, while a moderate inertia force ($a_{\max} = 0.15g$) is being applied to

the right of the bridge. In this case, the crust is weak and soft with a thickness of only 1.8 m, and the liquefied sand layer is 2.6 m thick.

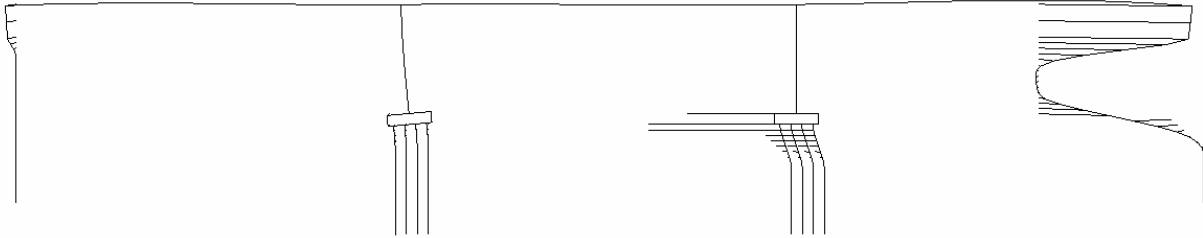


Figure 3: Deformations at the end of an analysis with very strong tall piers and thin and weak nonliquefiable crust and spreading occurring at the right side (deformations are amplified by a factor of 10.0).

As a result of the lateral spreading at the right side of the bridge, the entire bridge is moving about 100mm to the left at 2.0 m of maximum ground displacements (end of the analysis). The lateral spreading at the right pier is shifting the bottom of the right pier (right pile cap) by almost the same amount of top of the piers to the left. Therefore, similar to the analysis in Figure 2, there is not much curvature demand in the right pier and the pier stays intact, while the piles supporting the pier have reached a curvature ductility of 5 at the end of analyses (2.0 m of maximum ground displacement).

On the other hand, the pile cap of the left pier has not spread and is shifting 25mm to the left while rotating between 0.5 to 1.0 % in the counter-clockwise direction. While the mobilized drift (~ 0.75%) in these older piers is expected to at least yield the piers in bending, the left pier is also intact due to the modest rotation of the pile cap, which relieves the curvature demand on the pier. It can be deduced that drift ratio is not a very good measure of damage in the piers, in cases where some rotation is expected to occur at the bottom of the pier (pile cap) such as in the case of lateral spreading. That is the motivation for the authors to relate damage in the piers to the mobilized curvature which is a more fundamental measure of damage in the piers.

Two points should be noted at the end this section:

- 1) The reason why the latter analysis has performed so well relative to the previous analysis is the combined effect of the site having a weak, thin nonliquefiable crust above the liquefied sand layer (low demand), and high strength of piers (high resistance).
- 2) In both of these cases, the observed damage in the piers has been in the pier where lateral spreading was small or non-existent. This might seem counter-intuitive unless studied in detail in the context of global analyses. The global movement of the superstructure has reduced the demand in the spreading pier (in these cases, the right pier), while causing significant demand on the pier that is not spreading. A similar conclusion was found by Shin et al. (2008) using dynamic finite element models and global bridge analysis.

5. DISAGGREGATION OF PARAMETERS AND FRAGILITY CURVES

One of the advantages of performing Monte Carlo analyses is that the contribution of each of the input parameters can be investigated by disaggregating the results of the analyses to the input parameters. Disaggregation can be performed at different levels of performance of the bridge, and parameters with a stronger correlation are more important at the specified level of bridge performance. Since performance of a bridge is highly dependent on the performance of its piers, the results of disaggregation in this paper are presented at lateral ground displacements at which any of the piers of the bridges either reached a curvature ductility of 7 or failed in shear (Figure 4). These criteria are believed to cause very severe damage to the piers, and could likely result in collapse of the bridge. Even though the results of disaggregation at different levels of damage are not presented here, the trends remain the same. Also, due to limited space, the disaggregation

results are only presented for a few parameters.

As can be seen in Figure 4, the strongest correlation is observed between the lateral ground displacements required to reach a curvature ductility of 7 or a shear failure in the piers and the thickness of the natural nonliquefied crust overlying the liquefied sands. The spreading crust on top of the liquefied sand layer constitutes the largest contribution of the total load on to the structure and thus, it affects the performance of the bridge more severely. As can be observed in the figure, at a site with a thin natural crust (around 1m), this class of bridges can tolerate about 1m of lateral spreading displacements before experiencing severe damage at their piers, while at a site with a thick nonliquefied crust, on average only a few tenths of a meter of lateral displacements is sufficient to cause major damage at the piers in this class of bridges.

Unlike nonliquefied crust which contributes to a major portion of the total load, the liquefied sand layer is not a major contributor to the lateral spreading demands on the bridge. This phenomenon is also reflected in the results presented in Figure 4. As can be seen in the figure, there exists no trend between the performance of the bridge and the p -multiplier in liquefied sand. While many researchers have focused rigorously on the value of the p -multipliers in the liquefied sands, this parameter proved to be unimportant for the bridge models analyzed in this paper.

Figure 4 also shows that yield moment capacity of the piers and span length of the bridge has an important effect on the performance of the bridge. It is intuitive that a bridge with stronger piers should perform better than one with weaker piers under similar loading, while it might not be apparent why a longer-span bridge would perform better than a shorter-span bridge under lateral spreading demands. The key to understanding this trend is that longer-span bridges are typically designed with larger piers, which tend to have a higher moment capacity. Therefore, there is a direct positive correlation between moment capacity of piers and their span length that was built into the analyses.

It is also apparent from Figure 4 that while there are clear trends between the performance of the bridge and some of these parameters, there is significant scatter in the results at the entire range of each of the input parameters, which depicts that there is not a dominant parameter that by itself could provide accurate prediction of bridge vulnerability. However, combinations of parameters could be utilized to identify potentially vulnerable bridges (e.g., those with thick nonliquefiable crusts and weak piers).

Monte Carlo analyses could also be directly used to generate fragility curves at different level of structural performance. Figure 5, shows the fragility curves at four levels of pier performance (damage states). The first three damage states are defined as the maximum ground displacements required to cause curvature ductilities of 1, 2 and 4 in the piers, respectively. The fourth (most severe) damage state is defined as the maximum ground displacements required to either cause a curvature ductility of 7 in the piers or result in a shear failure (i.e. $V_{mobilized} > V_{capacity}$). As can be observed in the fragility curves, 50% of the bridges are expected to experience column failures with about 0.3m of lateral ground displacements, though some piers would sustain little damage at ground displacements as large as 2m.

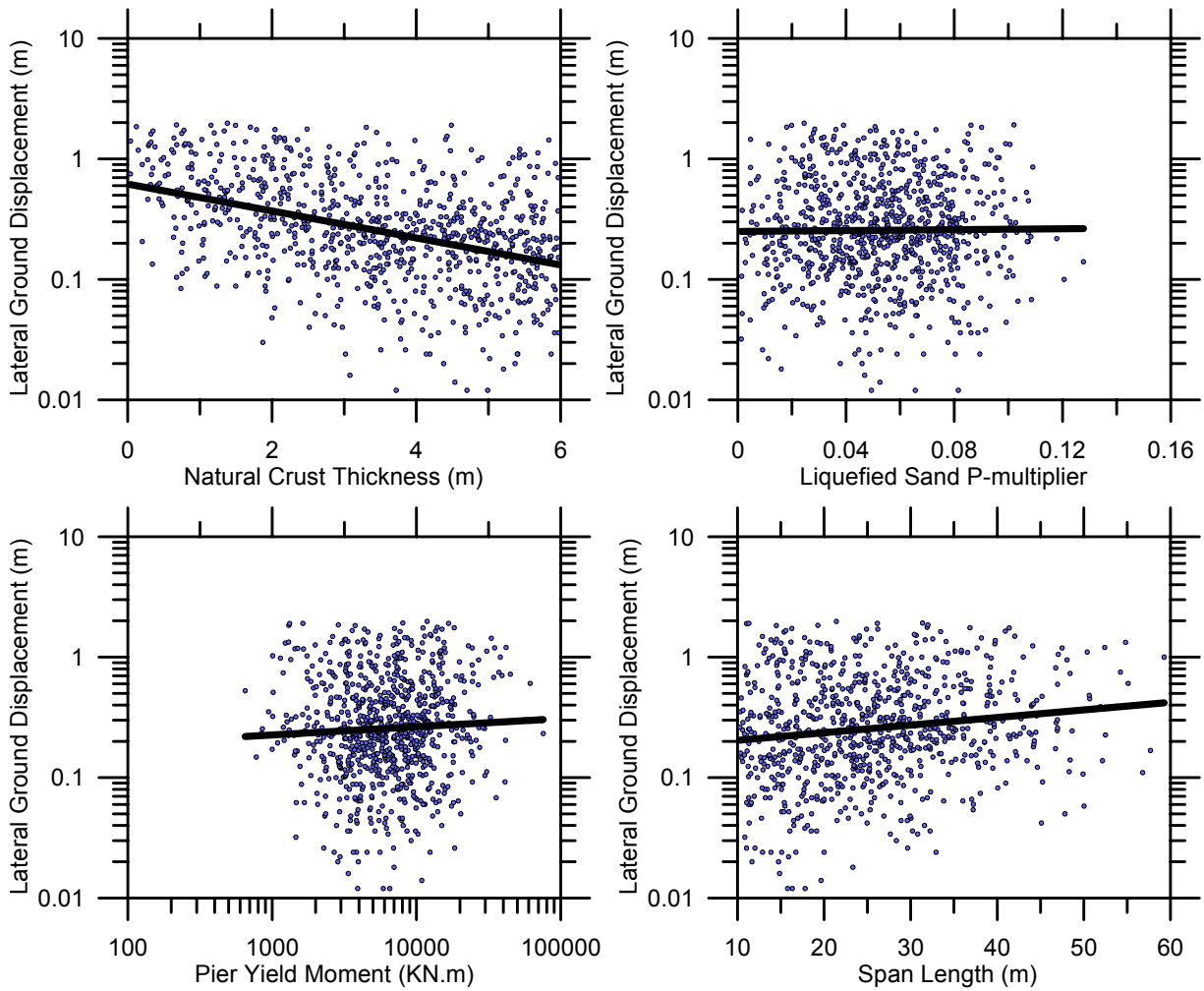


Figure 4: Disaggregation of the input parameters of interest versus maximum ground displacement at curvature ductility of 7 or shear failure in the piers

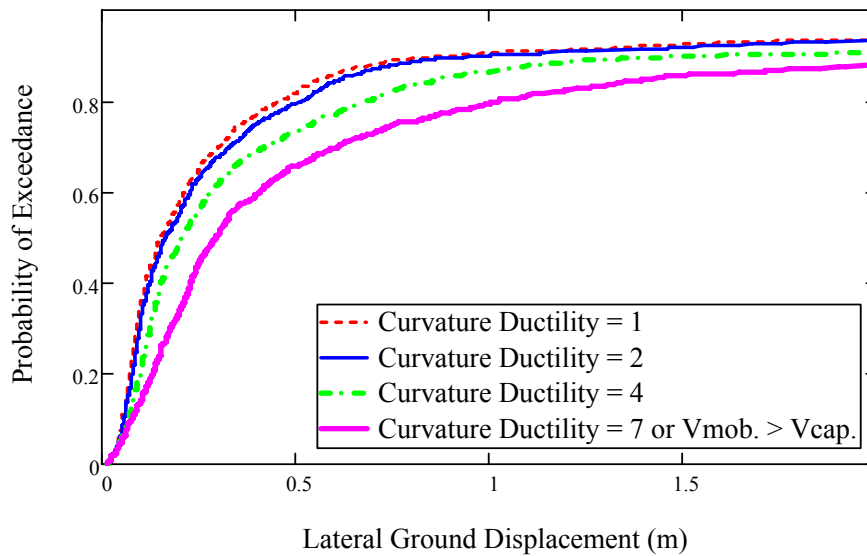


Figure 5: Fragility curves of older-vintage continuous bridges at different levels of damage

6. CONCLUSION

In this study, 950 global Monte Carlo analyses of older-vintage continuous bridges with monolithic abutments were performed with realistic variations in the input parameters using OpenSees finite element framework. Global analyses proved to be superior to component-wise analyses since the failure mechanisms observed in these analyses could not have been captured using component-wise analyses. The class of bridges studied here is found to be relatively fragile, while bridges located in sites with thinner and weaker nonliquefied crusts are expected to perform fairly well. Thickness of the natural nonliquefied crust and the moment capacity of the piers were two of the most important parameters in the performance of the bridge, while the p-multiplier in liquefied sand proved to be unimportant.

7. ACKNOWLEDGEMENTS

Funding for this project is provided by the Pacific Earthquake Engineering Research Center Lifelines program under project task No. 9C. Tom Shantz, Mark Yashinsky, Mark Mahan and Fadel Alameddine, provided valuable information and guidance for the project. The contents of this paper do not necessarily represent a policy of the funding agency or endorsement by the state or federal government.

REFERENCES

- Brandenberg, S.J., Boulanger, R.W., Kutter, B.L., and Chang, D. (2007). "Liquefaction induced softening of load transfer between pile groups and laterally spreading crusts." *J. of Geotech. Geoenviron. Eng.* 133(1). 91-103.
- Faris, A.T. (2004). "Probabilistic Models for Engineering Assessment of Liquefaction-Induced Lateral Spreading Displacements." *Ph.D. dissertation*, University of California, Berkeley.
- Mazzoni, S., McKenna, F., Scott, M.H., and Fenves, G.L. (2006). "Open system for earthquake engineering simulation user command-language manual." *Pacific earthquake engineering research center*, University of California, Berkeley. 465 p.
- Shin, H., Arduino, P., Kramer, S. L., and Mackie, K. (2008). "Seismic response of a typical highway bridge in liquefiable soil." *Proc. Geotechnical Earthquake Engineering and Soil Dynamics IV Conf.*, Sacramento, California, CD Rom.
- Transportation Research Board (TRB). (2002). *Comprehensive specification for the seismic design of bridges*. National Cooperative Highway Research Program (NCHRP) Report 472, National Research Council, 47 pp.